

# Momentum transfer dependence of kaon semileptonic form factor on $(10 \text{ fm})^4$ at the physical point

Takeshi Yamazaki,<sup>a,b,\*</sup> Ken-ichi Ishikawa,<sup>c</sup> Naruhito Ishizuka,<sup>b</sup>  
Yoshinobu Kuramashi,<sup>b</sup> Yusuke Namekawa,<sup>d</sup> Yusuke Taniguchi<sup>\*,b</sup>, Naoya Ukita<sup>b</sup> and  
Tomoteru Yoshié<sup>b</sup>

(PACS Collaboration)

<sup>a</sup>Faculty of Pure and Applied Sciences, University of Tsukuba, Tsukuba, Ibaraki 305-8571, Japan

<sup>b</sup>Center for Computational Sciences, University of Tsukuba, Tsukuba, Ibaraki 305-8577, Japan

<sup>c</sup>Core of Research for the Energetic Universe, Graduate School of Advanced Science and Engineering, Hiroshima University, Higashi-Hiroshima, 739-8526, Japan

<sup>d</sup>Education and Research Center for Artificial Intelligence and Data Innovation, Hiroshima University, Higashi-Hiroshima 739-8521, Japan

E-mail: [yamazaki@het.ph.tsukuba.ac.jp](mailto:yamazaki@het.ph.tsukuba.ac.jp)

We calculate the kaon semileptonic form factors using the two sets of the PACS10 configuration, whose physical volumes are more than  $(10 \text{ fm})^4$  at the physical point. The lattice spacings are 0.063 and 0.085 fm. The configurations were generated using the Iwasaki gauge action and  $N_f = 2 + 1$  stout-smearred nonperturbatively  $O(a)$ -improved Wilson quark action. From the momentum transfer dependence of the form factors, we evaluate the slope and curvature for the form factors at the zero momentum transfer. Furthermore, we calculate the phase space factor, which is used to obtain  $|V_{us}|$  through the kaon semileptonic decay. These results are compared with previous lattice results and experimental values.

*The 39th International Symposium on Lattice Field Theory,  
8th-13th August, 2022,  
Rheinische Friedrich-Wilhelms-Universität Bonn, Bonn, Germany*

\*Yusuke Taniguchi passed away on July 22, 2022, while this work was in progress.

\*Speaker

## 1. Introduction

A violation of the unitarity of the Cabibbo-Kobayashi-Maskawa (CKM) matrix implies the existence of physics beyond the standard model. In the first row of the CKM matrix, a  $2.2\sigma$  violation is reported using the current values for the matrix elements,  $|V_{ud}|$ ,  $|V_{us}|$ , and  $|V_{ub}|$  [1]. To confirm whether this violation exists or not, it is important to reduce the uncertainty of the matrix elements.

The value of  $|V_{us}|$  can be determined through the kaon semileptonic ( $K_{\ell 3}$ ) decay process. The  $K_{\ell 3}$  decay rate  $\Gamma_{K_{\ell 3}}$  is related to  $|V_{us}|$  as,

$$\Gamma_{K_{\ell 3}} = C_{K_{\ell 3}} (|V_{us}| f_+(0))^2 I_K^\ell, \quad (1)$$

where  $C_{K_{\ell 3}}$  is a known factor including the electromagnetic and SU(2) breaking corrections, and  $f_+(0)$  is the  $K_{\ell 3}$  form factor at zero momentum transfer  $q^2 = 0$ . The phase space integral  $I_K^\ell$  of the lepton  $\ell$  is usually calculated from the shape of the experimental  $K_{\ell 3}$  form factors. The value of  $f_+(0)$  needs to be determined from a nonperturbative calculation of the strong interaction, such as lattice QCD.

Precise values of  $f_+(0)$  were provided by various lattice QCD calculations [2–9] including ours [10]. Recently we report updates of our calculation in Ref. [11], where  $f_+(0)$  in the continuum limit is obtained using the two ensembles of the PACS10 configuration generated on more than  $(10 \text{ fm})^4$  volumes at the physical point. Since we evaluate the form factors as a function of  $q^2$ , in this report, we discuss physical quantities obtained from the  $q^2$  dependence of the form factors, which are the slope and curvature of the form factors at  $q^2 = 0$ , and also the phase space integral  $I_K^\ell$  in Eq. (1). Almost all results in this report were already presented in Ref. [11].

## 2. Result

The Iwasaki gauge action and the nonperturbatively improved Wilson quark action with the six-stout link smearing [12] are utilized to generate the PACS10 configuration, which has more than  $(10 \text{ fm})^4$  volume at the physical point. The details of the configuration generations are explained in Refs. [13] and [14] for the finer and coarser lattice spacings, respectively. The same quark action is employed in the measurement of the  $K_{\ell 3}$  form factors. The simulation parameters at each lattice spacing are tabulated in Table 1 including the masses for  $\pi$  and  $K$ ,  $M_\pi$  and  $M_K$ .

In this work we calculate the two  $K_{\ell 3}$  form factors,  $f_+(q^2)$  and  $f_0(q^2)$ , from the  $K_{\ell 3}$  3-point functions. Through the matrix element extracted from the 3-point functions,  $f_+(q^2)$  is defined by

$$\langle \pi(\vec{p}_\pi) | V_\mu | K(\vec{p}_K) \rangle = (p_K + p_\pi)_\mu f_+(q^2) + (p_K - p_\pi)_\mu f_-(q^2), \quad (2)$$

where  $q^2$  is the momentum transfer squared and  $V_\mu$  is the weak vector current. Another form factor  $f_0(q^2)$  is defined by  $f_+(q^2)$  and  $f_-(q^2)$  as,

$$f_0(q^2) = f_+(q^2) + \frac{-q^2}{m_K^2 - m_\pi^2} f_-(q^2). \quad (3)$$

The calculation of the 3-point functions is carried out using the local and conserved vector currents. Thus, we have two form factor data obtained from the local and conserved currents at

**Table 1:** Simulation parameters of the PACS10 configurations at the two lattice spacings. The bare coupling ( $\beta$ ), lattice size ( $L^3 \cdot T$ ), physical spatial extent ( $L[\text{fm}]$ ), lattice spacing ( $a[\text{fm}]$ ), the number of the configurations ( $N_{\text{conf}}$ ), and pion and kaon masses ( $m_\pi, m_K$ ) are tabulated.

$\beta$	$L^3 \cdot T$	$L[\text{fm}]$	$a[\text{fm}]$	$N_{\text{conf}}$	$m_\pi[\text{MeV}]$	$m_K[\text{MeV}]$
2.00	160 <sup>4</sup>	10.1	0.063	20	138	505
1.82	128 <sup>4</sup>	10.9	0.085	20	135	497

each lattice spacing. The local vector current is renormalized by the renormalization factor  $Z_V = 1/\sqrt{F_\pi^{\text{bare}}(0)F_K^{\text{bare}}(0)}$ . The two form factors,  $F_\pi^{\text{bare}}(0)$  and  $F_K^{\text{bare}}(0)$ , are the unrenormalized electromagnetic form factors for  $\pi$  and  $K$  at  $q^2 = 0$  with the local vector current.

## 2.1 Form factors

The data for  $f_+(q^2)$  and  $f_0(q^2)$  at finite lattice spacings are presented in Fig. 1 as a function of  $q^2$ . The figure contains the data calculated from the local and conserved currents at the two lattice spacings. Thanks to the huge volume of the PACS10 configurations, we obtain several data near the  $q^2 = 0$  region, which stabilize a  $q^2$  interpolation of the form factors to  $q^2 = 0$ . The lattice spacing dependence of the conserved current data is larger than that of the local current data, especially in  $f_+(q^2)$ .

We carry out simultaneous  $q^2$  interpolation and continuum extrapolation using all the data we calculated: the two form factors  $f_+(q^2)$  and  $f_0(q^2)$  with the local and conserved currents at the two lattice spacings. The fit form is based on the NLO SU(3) ChPT formula [15, 16], and we add correction terms corresponding to finite lattice spacing effects by introducing functions  $g_+^{\text{cur}}(q^2, a)$  and  $g_0^{\text{cur}}(q^2, a)$ . The superscript “cur” expresses the local or conserved vector currents. The fit forms are given by

$$f_+^{\text{cur}}(q^2) = 1 - \frac{4}{F_0^2} L_9 q^2 + K_+(q^2) + c_0 + c_2^+ q^4 + g_+^{\text{cur}}(q^2, a), \quad (4)$$

$$f_0^{\text{cur}}(q^2) = 1 - \frac{8}{F_0^2} L_5 q^2 + K_0(q^2) + c_0 + c_2^0 q^4 + g_0^{\text{cur}}(q^2, a). \quad (5)$$

The NLO functions  $K_+(q^2)$  and  $K_0(q^2)$  are described in Refs. [15, 16]. The pion decay constant in the chiral limit  $F_0 = 0.11205$  GeV is employed. We choose three types of  $g_{+,0}^{\text{cur}}(q^2, a)$ , called fit A, B, and C, to investigate a systematic error of the fit results, whose explicit forms are described in Ref. [11].

A typical example of the simultaneous fit results is presented in Fig. 1 by dashed and dot-dashed curves, which are obtained with the fit A form. From the fit results, the form factors in the continuum limit are obtained as a function of  $q^2$  presented in Fig. 2. In this report, we will discuss physical quantities obtained from the  $q^2$  dependence of the form factors. We note that the result of  $f_+(0)$  and value of  $|V_{us}|$  determined with our  $f_+(0)$  were discussed in Ref. [11].

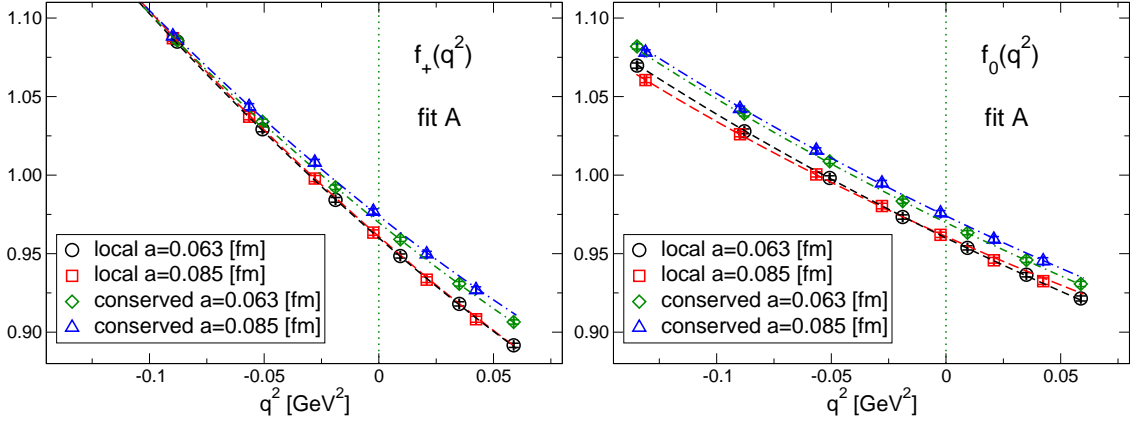


**Figure 1:** The  $K_{\ell 3}$  form factors  $f_+(q^2)$  and  $f_0(q^2)$  as a function of  $q^2$  are plotted in the left and right panels, respectively. In each panel, the data with the local and conserved currents at the two lattice spacings are expressed by different symbols. The dashed and dot-dashed curves represent fit results from a simultaneous  $q^2$  interpolation and continuum extrapolation with fit A. This figure is reprinted from Ref. [11].

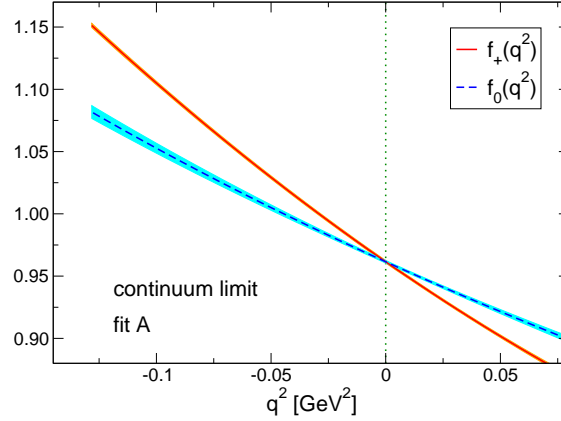


**Figure 2:** The  $K_{\ell 3}$  form factors  $f_+(q^2)$  and  $f_0(q^2)$  in the continuum limit using the fit A form for the continuum extrapolation. The error bands are only statistical error. This figure is reprinted from Ref. [11].

## 2.2 Slope and curvature

The slope and curvature of the  $K_{\ell 3}$  form factors at  $q^2 = 0$  are defined by

$$\lambda'_s = \frac{m_\pi^2}{f_+(0)} \left. \frac{df_s(q^2)}{d(-q^2)} \right|_{q^2=0}, \quad \lambda''_s = \frac{m_\pi^4}{f_+(0)} \left. \frac{d^2 f_s(q^2)}{d(-q^2)^2} \right|_{q^2=0}, \quad (6)$$

where  $s = +$  and  $0$ . Those quantities are evaluated from a  $q^2$  fit of the form factors at each lattice spacing and vector current data. Figure 3 shows the lattice spacing dependence of  $\lambda'_+$  and  $\lambda'_0$  with the two current data. For  $\lambda'_+$  in the left panel, the two current data have a different dependence on the lattice spacing, which is similar to the one of  $f_+(0)$  [11]. The results in the continuum limit obtained from the three fits using fit A, B, C, explained in the last subsection, are stable in this quantity. In contrast to  $\lambda'_+$ , the two current data of  $\lambda'_0$  in the right panel almost agree with each other at both lattice spacings. Thus, the results in the continuum limit largely depend on the fit forms in

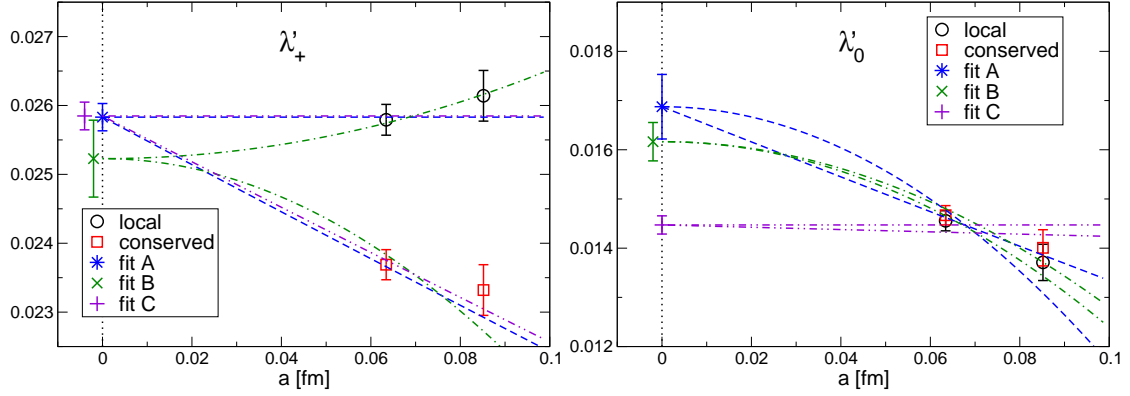


**Figure 3:** Lattice spacing dependence of  $\lambda'_+$  (left) and  $\lambda'_0$  (right). Circle and square symbols represent the results with the local and conserved current, respectively. Different curves correspond to fit results using different fit forms for the continuum extrapolation. This figure is reprinted from Ref. [11].

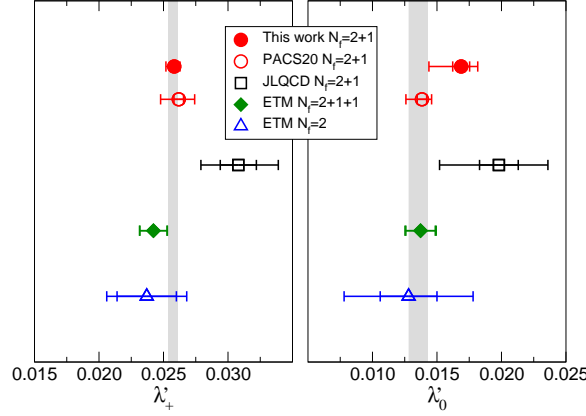


**Figure 4:** Comparison of our result of  $\lambda'_+$  (left) and  $\lambda'_0$  (right) with previous lattice results [6, 8, 10, 17] denoted by different symbols. The closed (open) symbols represent results in the continuum limit (at a finite lattice spacing). The experimental value [18] with one standard deviation is also presented by the gray band. The inner and outer errors express the statistical and total errors. The total error is evaluated by adding the statistical and systematic errors in quadrature. This figure is reprinted from Ref. [11].

the continuum extrapolation. A systematic error of the slopes is estimated from the differences of the fit results.

Our results for  $\lambda'_+$  and  $\lambda'_0$  are compared with previous lattice calculations [6, 8, 10, 17] in Fig. 4. Our results in the continuum limit are reasonably consistent with other lattice results and also the experimental values [18] expressed by the gray band. It is noted that our result of  $\lambda'_0$  has a larger systematic error than that of our previous calculation using the coarser lattice spacing configuration denoted by the open circle, because in the previous calculation the systematic error of a finite lattice spacing effect is estimated by an order counting.

A similar lattice spacing dependence to that of  $\lambda'_0$  is seen in both the curvatures, so that the extrapolated results largely depend on the fit forms. In Fig. 5, the results in the continuum limit are compared with our previous calculation [10], the experimental value evaluated with the dispersive representation [19], and the average of the experimental results [20]. Our continuum results agree

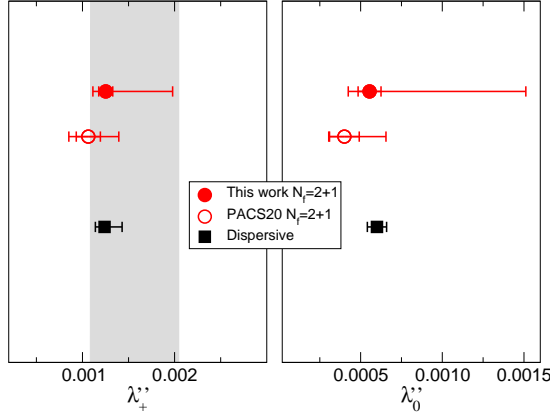


**Figure 5:** Comparison of our result of  $\lambda''_+$  (left) and  $\lambda''_0$  (right) in the continuum limit with our previous results [10] at the coarser lattice spacing and the experimental value evaluated with the dispersive representation [19]. The gray band corresponds to the average of the experimental results [20]. The inner and outer errors express the statistical and total errors. The total error is evaluated by adding the statistical and systematic errors in quadrature. This figure is reprinted from Ref. [11].

with those results, albeit our results have larger errors.

### 2.3 Phase space integral

The phase space integral  $I_K^\ell$  in Eq. (1) is defined by an integral of the form factors [21] as,

$$I_K^\ell = \int_{m_\ell^2}^{t_{\max}} dt \frac{\lambda^{3/2}}{M_K^8} \left(1 + \frac{m_\ell^2}{2t}\right) \left(1 - \frac{m_\ell^2}{t}\right)^2 \left(\overline{F}_+^2(t) + \frac{3m_\ell^2 \Delta_{K\pi}^2}{(2t + m_\ell^2)\lambda} \overline{F}_0^2(t)\right), \quad (7)$$

where  $t = -q^2$ ,  $t_{\max} = (M_K - M_\pi)^2$ ,  $\lambda = (t - (M_K + M_\pi)^2)(t - t_{\max})$ ,  $\Delta_{K\pi} = M_K^2 - M_\pi^2$ ,  $m_\ell$  is the mass of the lepton  $\ell$ , and  $\overline{F}_s(t) = f_s(-t)/f_+(0)$  with  $s = +$  and  $0$ . We evaluate  $I_{K^0}^\ell$  and  $I_{K^+}^\ell$  for  $\ell = e, \mu$  using  $(M_K, M_\pi) = (m_{K^0}, m_{\pi^-})$  and  $(m_{K^+}, m_{\pi^0})$ , respectively.

The results of  $I_K^\ell$  calculated with our form factors in the continuum limit are shown in Fig. 6 for each lepton. While our results have large systematic errors coming from the fit form dependence in the continuum extrapolations, those results are consistent with the experimental values using the form factors in the dispersive representation [20].

The value of  $|V_{us}|$  is determined using our result of  $I_K^\ell$  for six  $K_{\ell 3}$  decay processes. The experimental value of  $|V_{us}|f_+(0)\sqrt{I_K^\ell}$  in each decay process is obtained using the experimental inputs and correction factors in Refs. [20, 22–25]. Figure 7 shows that the six values of  $|V_{us}|$  are consistent within the total error evaluated using the lattice and experimental errors. Their weighted average with the experimental error is also plotted.

The value of  $|V_{us}|$  from the average of the six decay processes is compared with the previous results using  $f_+(0)$  [4–6, 8–10] including this calculation [11] as shown in Fig. 8. The result using  $I_K^\ell$  agrees with that using  $f_+(0)$  in this work within the total error. It is also reasonably consistent with other previous results and those determined from the kaon leptonic ( $K_{\ell 2}$ ) decay using  $F_K/F_\pi$  in our calculation and in PDG22 [1]. On the other hand, our result with  $I_K^\ell$  is  $4\sigma$  ( $2\sigma$ ) away from

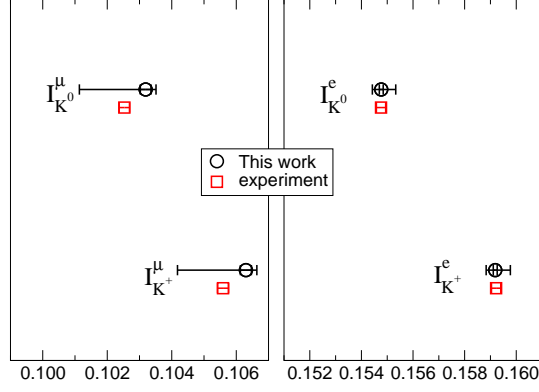


**Figure 6:** Results of the phase space integral evaluated from our form factors for the four channels. The experimental values [20] are also plotted. The inner and outer errors of the circle symbols express the statistical and total errors. The total error is evaluated by adding the statistical and systematic errors in quadrature.

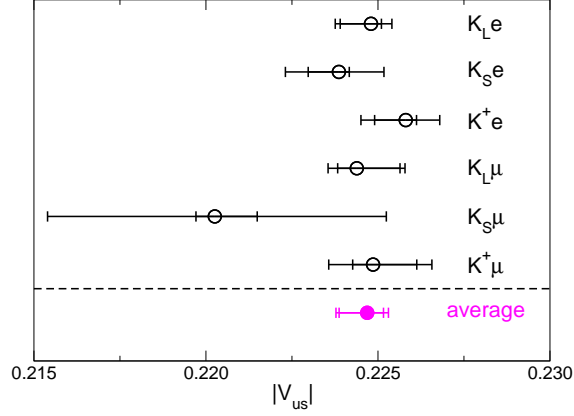


**Figure 7:** Values of  $|V_{us}|$  determined from our result of the phase space integral in the six decay processes. The average of those values is also plotted. The inner and outer errors express the lattice QCD and total errors. The total error is evaluated by adding the errors in the lattice QCD and experiment in quadrature.

the value determined through the CKM unitarity using  $|V_{ud}|$  in Ref. [26] ([27]), which is shown by the light blue (gray) band in the figure.

To clarify the difference, it is important to reduce the uncertainty in our calculation. As in our result of  $f_+(0)$ , the largest error in the  $I_K^\ell$  result stems from the fit form dependence in the continuum extrapolation. This systematic error could be largely reduced, if data at a smaller lattice spacing is added in the continuum extrapolation. It is an important future work in our calculation. To do this, we are generating the third PACS10 configuration at a smaller lattice spacing.

### 3. Summary

We have calculated the  $K_{\ell 3}$  form factors in the  $N_f = 2 + 1$  lattice QCD on large volumes at the physical point. Using the form factors at the two lattice spacings, we have carried out simultaneous  $q^2$  interpolation and continuum extrapolation of the form factors to obtain  $q^2$  dependent form

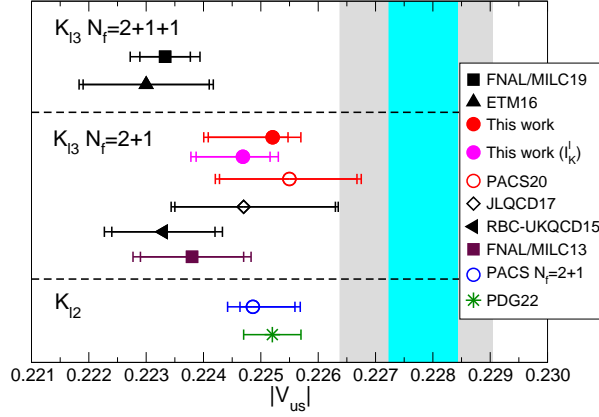


**Figure 8:** Comparison of  $|V_{us}|$  using our result of  $I_K^\ell$  with previous results using  $f_+(0)$  [4–6, 8–11].  $|V_{us}|$  determined from the  $K_{\ell 2}$  decay are also plotted using  $F_K/F_\pi$  in our calculation and PDG22 [1]. The closed (open) symbols represent results in the continuum limit (at a finite lattice spacing). The inner and outer errors express the lattice QCD and total errors. The total error is evaluated by adding the errors in the lattice QCD and experiment in quadrature. The value of  $|V_{us}|$  determined from the unitarity of the CKM matrix using  $|V_{ud}|$  in Refs. [26] and [27] are presented by the light blue and gray bands, respectively.

factors in the continuum limit. From the  $q^2$  dependence of the form factors, the slope and curvature at  $q^2 = 0$  are evaluated. Those results are consistent with the previous lattice calculations and the experimental values. The phase space integral is also evaluated using our form factors in the continuum limit. The value of  $|V_{us}|$  determined using the results of the phase space integral is consistent with our result with  $f_+(0)$  in the same calculation, and reasonably agrees with the previous results. Since our error is dominated by the systematic error coming from the fit form dependence in the continuum extrapolation, the reduction of this error is an important future direction. For this purpose, the third PACS10 configuration is generated at a smaller lattice spacing. We plan to calculate the  $K_{\ell 3}$  form factors using the configuration.

## Acknowledgments

Numerical calculations in this work were performed on Oakforest-PACS in Joint Center for Advanced High Performance Computing (JCAHPC) under Multidisciplinary Cooperative Research Program of Center for Computational Sciences, University of Tsukuba. This research also used computational resources of Oakforest-PACS by Information Technology Center of the University of Tokyo, and of Fugaku by RIKEN CCS through the HPCI System Research Project (Project ID: hp170022, hp180051, hp180072, hp180126, hp190025, hp190081, hp200062, hp200167, hp210112, hp220079). The calculation employed OpenQCD system<sup>1</sup>. This work was supported in part by Grants-in-Aid for Scientific Research from the Ministry of Education, Culture, Sports, Science and Technology (Nos. 18K03638, 19H01892). This work was supported by the JLDG constructed over the SINET5 of NII.

<sup>1</sup><http://luscher.web.cern.ch/luscher/openQCD/>



## References

- [1] PARTICLE DATA GROUP collaboration, *Review of Particle Physics*, [\*PTEP\* \*\*2022\*\* \(2022\) 083C01](#).
- [2] FERMILAB LATTICE, MILC collaboration, *Kaon semileptonic vector form factor and determination of  $|V_{us}|$  using staggered fermions*, [\*Phys. Rev.\* \*\*D87\*\* \(2013\) 073012 \[1212.4993\]](#).
- [3] RBC-UKQCD collaboration,  *$K(l3)$  semileptonic form-factor from 2+1 flavour lattice QCD*, [\*Phys. Rev. Lett.\* \*\*100\*\* \(2008\) 141601 \[0710.5136\]](#).
- [4] RBC-UKQCD collaboration, *The kaon semileptonic form factor with near physical domain wall quarks*, [\*JHEP\* \*\*08\*\* \(2013\) 132 \[1305.7217\]](#).
- [5] RBC-UKQCD collaboration, *The kaon semileptonic form factor in  $N_f = 2 + 1$  domain wall lattice QCD with physical light quark masses*, [\*JHEP\* \*\*06\*\* \(2015\) 164 \[1504.01692\]](#).
- [6] JLQCD collaboration, *Chiral behavior of  $K \rightarrow \pi l \nu$  decay form factors in lattice QCD with exact chiral symmetry*, [\*Phys. Rev.\* \*\*D96\*\* \(2017\) 034501 \[1705.00884\]](#).
- [7] FERMILAB LATTICE, MILC collaboration, *Determination of  $|V_{us}|$  from a lattice-QCD calculation of the  $K \rightarrow \pi l \nu$  semileptonic form factor with physical quark masses*, [\*Phys. Rev. Lett.\* \*\*112\*\* \(2014\) 112001 \[1312.1228\]](#).
- [8] ETM collaboration,  *$K \rightarrow \pi$  semileptonic form factors with  $N_f = 2 + 1 + 1$  twisted mass fermions*, [\*Phys. Rev.\* \*\*D93\*\* \(2016\) 114512 \[1602.04113\]](#).
- [9] FERMILAB LATTICE, MILC collaboration,  *$|V_{us}|$  from  $K_{\ell 3}$  decay and four-flavor lattice QCD*, [\*Phys. Rev.\* \*\*D99\*\* \(2019\) 114509 \[1809.02827\]](#).
- [10] PACS collaboration,  *$K_{l3}$  form factors at the physical point on a  $(10.9\text{ fm})^3$  volume*, [\*Phys. Rev. D\* \*\*101\*\* \(2020\) 094504 \[1912.13127\]](#).
- [11] PACS collaboration,  *$K_{\ell 3}$  form factors at the physical point: Toward the continuum limit*, [\*Phys. Rev. D\* \*\*106\*\* \(2022\) 094501 \[2206.08654\]](#).
- [12] C. Morningstar and M.J. Peardon, *Analytic smearing of  $SU(3)$  link variables in lattice QCD*, [\*Phys. Rev.\* \*\*D69\*\* \(2004\) 054501 \[hep-lat/0311018\]](#).
- [13] PACS collaboration, *Hadronic vacuum polarization contribution to the muon  $g - 2$  with 2+1 flavor lattice QCD on a larger than  $(10\text{ fm})^4$  lattice at the physical point*, [\*Phys. Rev. D\* \*\*100\*\* \(2019\) 034517 \[1902.00885\]](#).
- [14] PACS collaboration, *Finite size effect on pseudoscalar meson sector in 2+1 flavor QCD at the physical point*, [\*Phys. Rev.\* \*\*D99\*\* \(2019\) 014504 \[1807.06237\]](#).
- [15] J. Gasser and H. Leutwyler, *Low-Energy Expansion of Meson Form-Factors*, [\*Nucl. Phys.\* \*\*B250\*\* \(1985\) 517](#).

- [16] J. Gasser and H. Leutwyler, *Chiral Perturbation Theory: Expansions in the Mass of the Strange Quark*, *Nucl. Phys.* **B250** (1985) 465.
- [17] ETM collaboration,  *$K \rightarrow \pi l \nu$  Semileptonic Form Factors from Two-Flavor Lattice QCD*, *Phys. Rev.* **D80** (2009) 111502 [0906.4728].
- [18] M. Moulson, *Experimental determination of  $V_{us}$  from kaon decays*, *PoS CKM2016* (2017) 033 [1704.04104].
- [19] V. Bernard, M. Oertel, E. Passemar and J. Stern, *Dispersive representation and shape of the  $K(l3)$  form factors: Robustness*, *Phys. Rev.* **D80** (2009) 034034 [0903.1654].
- [20] FLAVIANET WORKING GROUP ON KAON DECAYS collaboration, *An Evaluation of  $|V_{us}|$  and precise tests of the Standard Model from world data on leptonic and semileptonic kaon decays*, *Eur. Phys. J.* **C69** (2010) 399 [1005.2323].
- [21] H. Leutwyler and M. Roos, *Determination of the Elements  $V(us)$  and  $V(ud)$  of the Kobayashi-Maskawa Matrix*, *Z. Phys.* **C25** (1984) 91.
- [22] C.-Y. Seng, D. Galviz, W.J. Marciano and U.-G. Meißner, *Update on  $|V_{us}|$  and  $|V_{us}/V_{ud}|$  from semileptonic kaon and pion decays*, *Phys. Rev. D* **105** (2022) 013005 [2107.14708].
- [23] C.-Y. Seng, D. Galviz, M. Gorchtein and U.-G. Meißner, *Full  $K_{\ell 3}$  radiative corrections and implications on  $|V_{us}|$* , [2203.05217](#).
- [24] C.-Y. Seng, D. Galviz, M. Gorchtein and U.G. Meißner, *High-precision determination of the  $Ke3$  radiative corrections*, *Phys. Lett. B* **820** (2021) 136522 [2103.00975].
- [25] C.-Y. Seng, D. Galviz, M. Gorchtein and U.-G. Meißner, *Improved  $K_{e3}$  radiative corrections sharpen the  $K_{\mu 2}$ – $K_{l3}$  discrepancy*, *JHEP* **11** (2021) 172 [2103.04843].
- [26] C.-Y. Seng, M. Gorchtein, H.H. Patel and M.J. Ramsey-Musolf, *Reduced Hadronic Uncertainty in the Determination of  $V_{ud}$* , *Phys. Rev. Lett.* **121** (2018) 241804 [1807.10197].
- [27] J.C. Hardy and I.S. Towner, *Superaligned  $0^+ \rightarrow 0^+$  nuclear  $\beta$  decays: 2020 critical survey, with implications for  $V_{ud}$  and CKM unitarity*, *Phys. Rev. C* **102** (2020) 045501.